Rise and Deformation Modeling of Single Droplet Motion in Yield Stress Fluids by Using Aspect Ratio and Dimensionless Numbers

Shaobai, Li*[+] ; Xuelin, Sun; Bhusal, Manju Lata

College of Energy and Environment, Shenyang Aerospace University, Shenyang 110000, P.R. CHINA

ABSTRACT: *The motion of a single droplet rising in quiescent yield stress fluids was investigated experimentally. By using a high-speed camera to follow the rising droplet, the images of the recorded frames were digitized and analyzed using MATLAB, and the aspect ratio and terminal velocity of the droplets were obtained. The results show that the droplet aspect ratio decreases with the increase of dimensionless numbers such as Eötvös number and Tadaki number, and the droplet gradually changes from spherical to ellipsoidal. The larger the yield stress, the larger the Bingham number, which limits the lateral stretching of the droplet, and the droplet shows a spherical shape. The experimental drag coefficient and aspect ratio were compared with correlations in literature, and the comparison showed that these correlations do not give fully satisfactory results in predicting the drag coefficient and aspect ratio of droplet rising in yield stress fluid, showing a big relative error. Therefore, two new empirical correlations were proposed to predict the aspect ratio and the drag coefficient, respectively. It was found that the calculated results by the present correlation agree well with the experimental data.*

KEYWORDS: *Yield stress fluids*; *Droplet*; *Velocity*; *Shape*; *Drag coefficient*.

INTRODUCTION

Droplets widely exist in liquid-liquid two-phase systems, such as petroleum drilling [1], phase transfer catalysis [2], liquid-liquid extraction [3,4], etc. Understanding the motion behavior of droplets in the fluid plays an important role in the process optimization design. Although most of the droplet motion involved in the above industrial processes is the motion of a droplet swarm, the understanding of the shape, velocity, and drag coefficient of a single droplet is essential for understanding the motion of multiple droplets [5].

At present, the research on droplet motion behavior is mainly aimed at the droplet in Newtonian fluids, and the motion parameters investigated include droplet shape, terminal velocity, and drag coefficient [6-8]. Researchers have found that droplet motion is affected by viscous force, inertial force, surface tension, and buoyancy. In addition, droplet geometry and liquid-liquid two-phase properties also have a certain influence on droplet formation, shape, and velocity [9-14]. In the past, Taylor [9] found through theoretical derivation that there was a certain connection between the droplet shape and the Reynolds number. As the Reynolds number increased, the droplet

***** *To whom correspondence should be addressed.*
+ E-mail: lishaobai1982@163.com
1021-9986/2023/2/472-485 14/$/6.04

the droplet gradually changed from a spherical shape to a flat shape. Wairegi and Grace [10] researched the relationship between the physical properties of the continuous liquid phase and droplet shape through experiments and found that droplet shape was also closely related to Weber number. *Liu et al.* [11] studied the influence of viscosity ratio, density ratio, and Eötvös number on the motion speed and shape change of rising droplets in stationary fluid, and found that viscosity ratio and Eötvös number had a great influence on droplet shape, while density ratio had a negligible influence on droplet shape, and the increase of Eötvös number would significantly improve the deformation degree of the droplet [12]. For droplets, besides the above motion parameters, the influence mechanism of terminal velocity is also complicated. The research of *Wegener et al.* [8] showed that with the increase of droplet diameter in water, the droplet terminal velocity would oscillate around a value, and its shape would also oscillate along with the velocity oscillation. In addition, the shear stress exerted by the surrounding fluid on the droplet will affect the interface of the droplet, resulting in the internal circulation of the droplet, and also affecting the terminal velocity of the droplet [13]. When mass transfer exists between the droplet phase and the continuous phase, the terminal velocity will also decrease to a certain extent [14]. However, the motion behavior of droplets in the liquid phase is much more complicated than that of bubbles and solid particles due to the influence of the viscosity ratio in a liquid-liquid system. The current understanding of droplet motion behavior is still limited, especially for non-Newtonian fluids due to the complex rheology.

Yield stress fluid is a kind of common non-Newtonian fluid, which is characterized by the fact that the material does not flow when the force is small and reflects the solid nature. Flow occurs only when the stress is greater than the yield stress [15]. Therefore, the small droplet cannot move and remain suspended when its buoyancy is less than the yield stress. As the droplet diameter increases, the droplet begins to move, but the fluid at a far distance from the droplet remains unyielding, resulting in the flow field around the droplet, the shape characteristics of the droplet, and the velocity of the droplet being very different from that in other fluids [16]. *Lavrenteva et al.* [17] studied the settlement behavior of tetrachloroethylene droplets in Carbopol solution. Under certain conditions, the wall effect increased the drag force of droplet motion, and droplets of the same volume had higher terminal velocity in a larger diameter tube. With the increase of droplet diameter and solution concentration, the droplet deforms from an asymmetric long ellipsoid into a tear droplet shape. *Sarabian et al.* [18] studied the effects of fluid viscosity, plasticity, and elasticity on particle motion by using numerical simulation. The drag of particles in yield stress fluid is divided into form drag (the drag component resulting from the distribution of the dynamic pressure on the sphere), viscous drag, and polymer drag. The form drag is dominant, and the total drag increases with the increase of yield stress. At present, only a few pieces of literature have reported relevant studies on yield stress fluids, and most of them are discussed from the determination of yield region and the general law of flow field. Studies on droplet movement behavior need to be supplemented. Relevant investigation can provide a theoretical basis for the optimization design of chemical-related processes.

In this paper, consideration is given to the upward motion of a single droplet in a yield stress fluid at a low Reynolds number. The shape and velocity of droplets were recorded by a high-speed camera, and the shape and velocity of a single droplet were obtained by Matlab image processing. The droplet shape was characterized by aspect ratio, and the variation of droplet shape with Reynolds number and Eötvös number was discussed. The accuracy of the model in predicting droplet drag coefficient was evaluated by comparing the experimental results with the mathematical model in the literature [19-22]. Based on a large number of experimental data, a correlation for the drag coefficient of a single droplet through a yield stress liquid was proposed. This correlation could represent the present experimental data with good accuracy.

EXPERIMENTAL SECTION

Materials

Carbopol 941 aqueous solutions with different concentrations were used as continuous phases. The concentration of Carbopol aqueous solution is low and the droplet velocity is also low. Therefore, the elastic effect of the continuous phase can be eliminated and only its yield stress can be retained [16, 17]. Soybean oil is used as a droplet phase (viscosity is 0.279 Pa·s). The preparation method of the Carbopol solution is as follows: Firstly, use an electronic balance to weigh an appropriate amount

of dried Carbopol powder, and add it to deionized water in batches. At the same time, use an electric stirrer to stir for 5 hours until the powder is completely dissolved. Adjust the pH of the solution to 7 by adding NaOH solution (1 mol/L). The solution is slowly poured through a glass funnel along the wall into a plexiglass tank and left to rest for 24 hours to ensure that the bubbles in the solution are completely removed.

Densities were measured using a densitometer (Anton Paar, DMA5000, Germany), which had an accuracy of ± 0.05 kg/m^3. Surface tensions were measured using a surface tension apparatus (DCAT21, data physics, Austria) with an accuracy of ± 0.001 mN/m. The rheological characteristics of Carbopol aqueous solutions were measured with the rheometer of Brookfield (Brookfield, DV-Ⅲ, USA) for shear rates ranging from 0.1-1000 s^{-1}. Different shear rates can be obtained by controlling the rotational speed of the paddle rotor, the standard deviation of the results is less than ± 1.0%. Carbopol aqueous solutions are an ideal yield stress fluid, and their rheology is well-described by the Herschel-Bulkley model [23]. For simple shear flow, the constitutive equation of the fluid can be expressed as

$$\tau = \tau_0 + k\dot{\gamma}^n \quad , \quad \tau > \tau_0 \tag{1}$$

$$\dot{\gamma} = 0 \quad , \quad \tau < \tau_0 \tag{2}$$

Therefore, the viscosity of the fluid is

$$\mu = \tau_0 / \dot{\gamma} + k\dot{\gamma}^{n-1} \tag{3}$$

To ensure the accuracy of the measurement results, the material was pre-sheared for 30 s before the measurement to eliminate the influence of the thixotropic effect. Measurements were made using a rotor with cruciform blades equipped with the rheometer [24]. Combined with the Herschel-Bulkley rheological model to calculate the relevant data.

The rheological properties and physical properties of experimental materials are shown in Table 1.

Apparatus

The experimental facility for measuring the motion of a droplet in yield stress fluids is sketched in Fig. 1 and includes two parts: droplet generation system and image acquisition system. The droplet generation system includes a plexiglass square measuring tank 0.15 m×0.15 m×1.3 m, a peristaltic pump, nozzles, and a pipeline system. Compared with the droplet size, the wall effect of the plexiglass tank can be ignored [25]. The droplet size is controlled by the peristaltic pump and the size of the nozzles. The inner diameters of nozzles are the following sizes: 0.86 mm, 1.05 mm, 1.30 mm, 2.40 mm, 3.80 mm, 5.80 mm. The image acquisition system included a high-speed video camera (Vision Research Phantom V611), background lamp, light diffuser, and computer. The experimental camera has a frame rate of 100fps and a resolution of 1024 × 768 pixels. For the experiment, pour soybean oil into the beaker and use a hose to connect the peristaltic pump to the nozzle. Start the peristaltic pump and adjust the appropriate flow rate and nozzle diameter to generate droplets of different sizes. Sufficient time (more than 1 hour) should be allowed between the formation of adjacent droplets to allow the solution to return to its initial state and avoid interference between droplets [16]. The images collected were processed by Matlab, and the equivalent diameter, aspect ratio, and terminal velocity of the droplet were obtained. Experiments were conducted at room temperature (25±1℃) under atmospheric pressure.

Image processing method

The droplet rises at a low speed and maintains an axisymmetric spherical or ellipsoidal shape without surface oscillation or violent droplet deformation. Therefore, the two-dimensional image can be used to represent the three-dimensional droplet shape. The video images were analyzed frame-by-frame, and the increment between successive positions of a droplet was measured against the calibrating scale. Assuming that the position of the center of gravity of the droplet in one frame is y_i that of the center of gravity in the next frame is y_{i+1}, and the time interval between two consecutive images is Δt, the instantaneous velocity U_b of the droplet can be obtained. When the instantaneous velocity error of the droplet in the two adjacent images is less than 10%, the droplet is considered to have reached terminal velocity U_T.

$$U_b = \frac{y_{i+1} - y_i}{\Delta t} \tag{4}$$

From the pumping rate of the peristaltic pump, the volume of the generated droplet can be obtained, and then the droplet equivalent diameter can be obtained. The equivalent diameter of the droplet is

$$d_e = \sqrt[3]{\frac{6V}{\pi}} \tag{5}$$

Table 1: Fluid physical property parameters.

Type of fluid	Yield stress τ_0(Pa)	Consistency coefficient k (Pa·s^n)	Power-law index n	Density ρ (kg·m^{-3})	Surface tension σ (mN·m^{-1})
0.25 wt% Carbopol aqueous solution	0.14	0.51	0.47	1099.15	57.326
0.275 wt% Carbopol aqueous solution	0.36	0.83	0.34	1104.11	60.011
0.325 wt% Carbopol aqueous solution	0.50	1.40	0.28	1110.09	62.586
0.5 wt% Carbopol aqueous solution	0.99	1.72	0.21	1113.24	64.141
Soybean oil	-	-	-	889.03	29.221

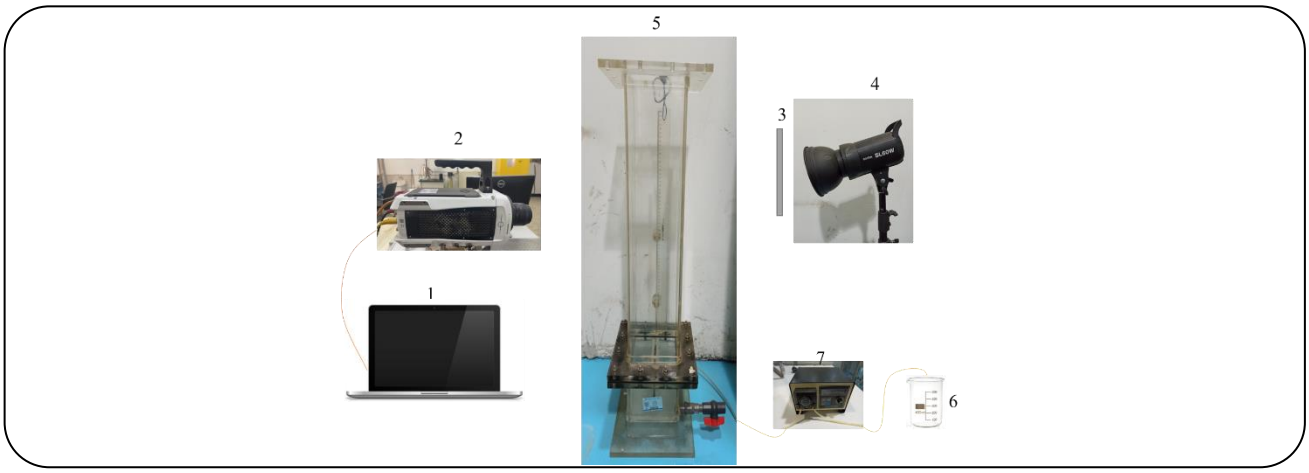

Fig. 1: Experimental setup diagram (1. computer, 2. high-speed camera, 3. light diffuser, 4. background lamp, 5. plexiglass tank, 6. beaker, 7. peristaltic pump)

Where V is the volume of the droplet.

The uncertainty analysis of the image processing results was carried out using the falling ball method. The sedimentation process of the stainless steel ball in the experimental fluid was recorded by a high-speed camera, and the volume of the stainless steel ball was obtained using MATLAB image processing. Comparing the measured volume with the actual volume shows that the overall error in measurement and image processing is less than 5%.

Definition of dimensionless numbers

The establishment of a droplet motion model is generally based on dimensional analysis, this paper chose the Reynolds number (the ratio of inertia force to viscous force), Eötvös number (the ratio of gravitational force to surface tension force), Weber number (the ratio of the inertial force to surface tension force), and Bingham number (the ratio of yield stress force to viscous force) as dimensionless parameters. It should be noted that the viscosity parameters in the dimensionless numbers above are constant values, whereas yield stress fluids have shear thinning properties and the viscosity varies with the shear rate. The dimensionless parameters were redefined according to the effective viscosity at the characteristic shear rate (U_b/d_e) [26]:

$$\mathrm{Re}^* = \frac{\mathrm{Re}}{1+\mathrm{Bn}} = \frac{\rho_C d_e U_T^{\,2}}{\tau_0 d_e + \mu U_T} \tag{6}$$

$$\mathrm{Eo}^* = \frac{\mathrm{Eo}}{1+\mathrm{Bn}} = \frac{(\rho_C - \rho_D) g d_e^{\,2} \mu U_T}{\sigma(\tau_0 d_e + \mu U_T)} \tag{7}$$

$$\mathrm{We}^* = \frac{\mathrm{We}}{1+\mathrm{Bn}} = \frac{\rho_C d_e \mu U_T^{\,3}}{\sigma(\tau_0 d_e + \mu U_T)} \tag{8}$$

$$\mathrm{Bn}^* = \frac{\mathrm{Bn}}{1+\mathrm{Bn}} = \frac{\tau_0 d_e}{\tau_0 d_e + \mu U_T} \tag{9}$$

RESULTS AND DISCUSSION

Droplet shape

The density difference between the continuous phase and the dispersed phase is small, and the yield stress and

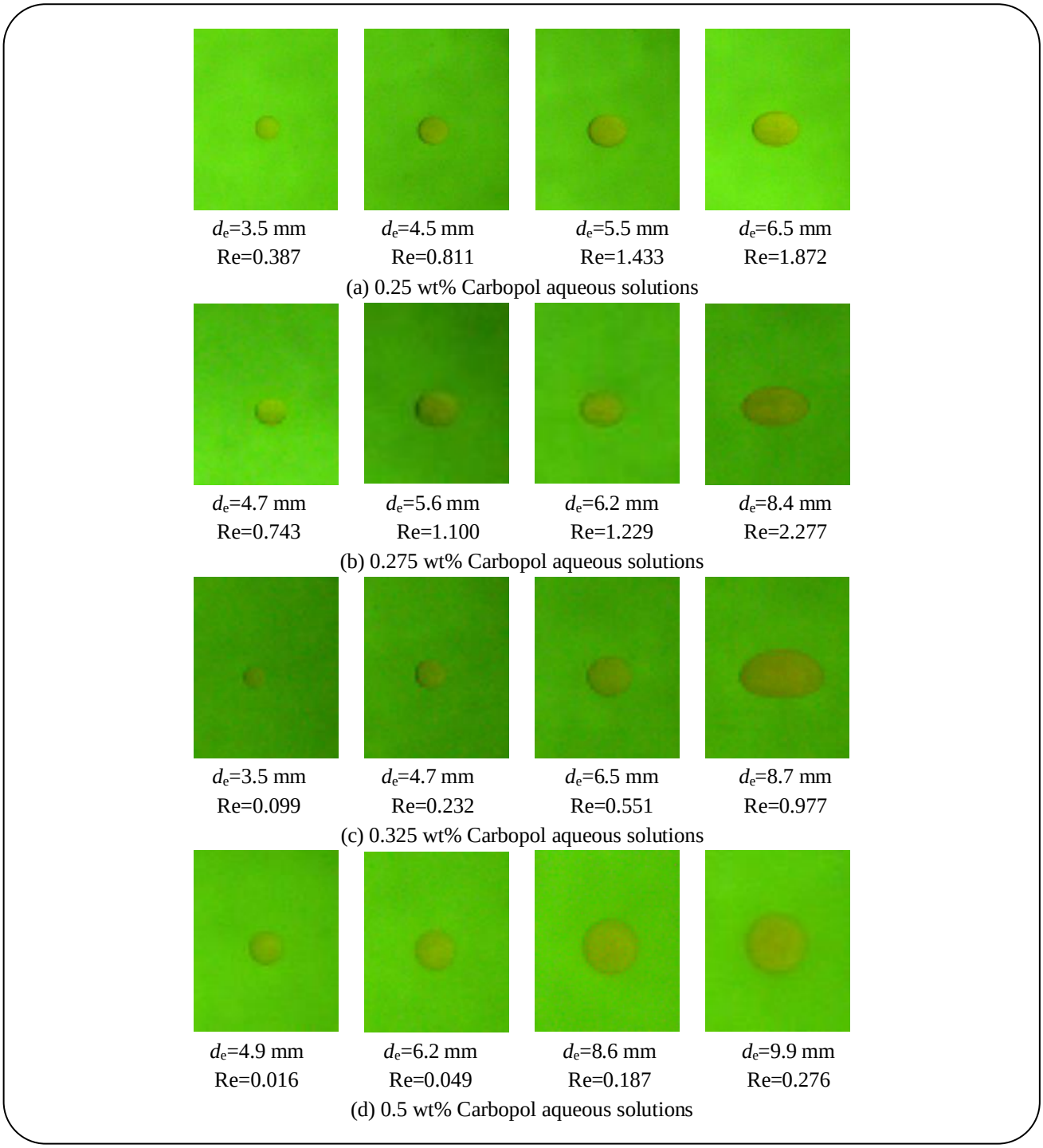

Fig.2: Droplet shapes in Carbopol aqueous solutions of different concentrations.

viscosity of the continuous phase are larger, leading to the lower velocity of the dispersed phase droplet. The droplet is spherical and ellipsoid in shape and keeps straight rising without surface oscillation. Fig. 2 shows the droplet image taken in the experiment.

Fig. 3 shows the distribution of droplet shape with Reynolds number and Eötvös number in the Carbopol solution. In low Reynolds number (Re < 1) fluids, viscous forces and surface tension dominate and droplet shapes are spherical, which is consistent with the conclusion of

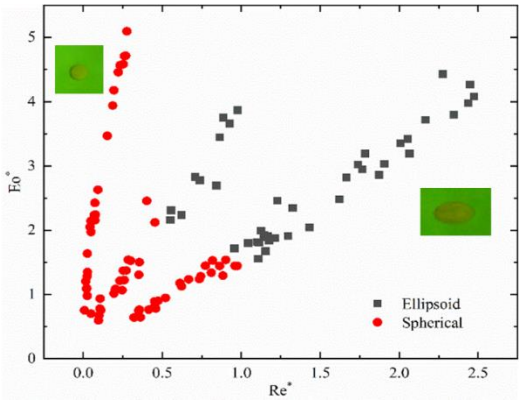

Fig. 3: Typical droplet shape diagram.

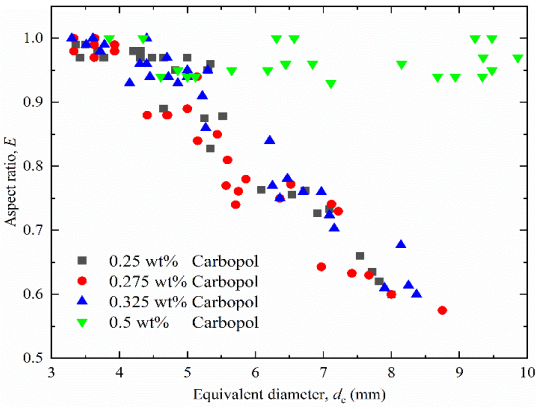

Fig.4: Droplet aspect ratio varies with an equivalent diameter.

Clift et al. [27]. When Reynolds number is greater than 1 and Eo > 1.5, the droplet shape is ellipsoidal, and the critical Eötvös number for droplet shape change in this experiment is smaller than the value given by Clift. The reason is that the Carbopol solution has obvious shear thinning and yield stress. With the increase of droplet velocity, the shear reduces the viscosity of the surrounding fluid. Inertial and viscous effects change the droplet from spherical to ellipsoid. When the droplet is in a state of fast motion, its shape change may be similar to Clift's conclusion, showing a ball cap shape. However, this phenomenon was not observed due to the small density difference between the droplet phase and the continuous phase and the large viscosity of the continuous phase.

Fig. 4 shows droplet aspect ratio changes with equivalent diameter in Carbopol solutions with different concentrations. When d_e < 4 mm, the aspect ratio is kept near 1, and the droplet is spherical. When d_e > 4 mm, in a low-concentration solution, due to the low viscosity of the solution, the viscous force is small, and the inertia force plays a dominant role. The aspect ratio of the droplet decreases with the increase of the diameter, and the droplet gradually deviates from the spherical shape and finally takes the shape of an ellipsoid or a spherical cap. In a high-concentration solution, the inertial force is small, and the viscous force plays a dominant role, and the lateral stretching of the droplet is restricted. The aspect ratio does not change significantly with the diameter of the droplet, and the droplet remains spherical.

Experimental studies have been carried out on the prediction of droplet aspect ratio. *Clift et al.* [27] proposed the aspect ratio correlation of droplets in Newtonian fluids:

$$E=\begin{cases}1 & Eo \le 0.4\\ \dfrac{1}{1+0.18(Eo-0.4)^{0.8}} & 0.4 < Eo < 8\end{cases} \quad (10)$$

Wellek et al. [28] proposed the correlation between the aspect ratio of droplet and Eötvös number in Newtonian fluids:

$$E=\frac{1}{1+0.163Eo^{0.757}} \quad (11)$$

Fig. 5 shows the changes in the aspect ratio with Eötvös number in different concentrations of solutions. It can be seen, when Eo < 1, the aspect ratio remains 1. When Eo > 1, the aspect ratio decreases with the increase of Eötvös number, and the droplet becomes ellipsoid gradually. However, the aspect ratio of the droplets fluctuated around 0.95 and the droplets remained spherical in 0.5 wt% Carbopol solution. Although *Wellek et al.* 's correlation showed a similar trend with the data, the consistency of the data was poor and the accuracy needed to be improved.

Tadaki et al. [29] proposed a new dimensionless number Ta to study the shape changes of bubbles in polluted Newtonian systems and pure water.

$$E=\begin{cases}0.24 & 16.5 < Ta\\ 2.52Ta^{-0.84} & 6 < Ta < 16.5\\ 1.48Ta^{-0.528} & 2 < Ta < 6\\ 1 & Ta < 2\end{cases} \quad (12)$$

Myint et al. [30] used the Tadaki number to predict the aspect ratio of silicone oil droplets in pure water and glycerol aqueous solution, and the results showed that

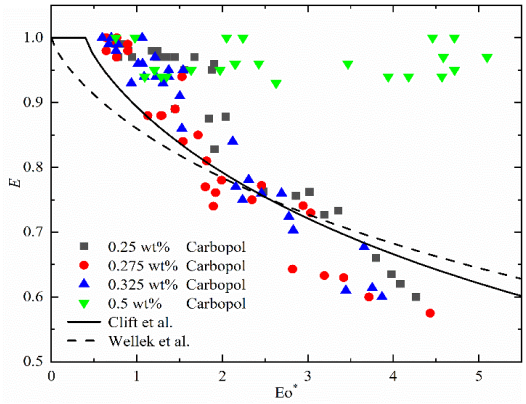

Fig. 5: Comparison of measured aspect ratio values with calculated values vs. Eötvös number.

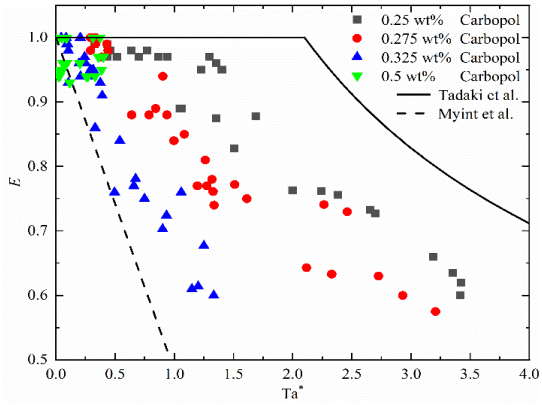

Fig. 6: Comparison of measured aspect ratio values with calculated values vs. Tadaki number.

under its experimental conditions, the accuracy of correlation using the Tadaki number was significantly higher than other dimensionless numbers.

$$E = 1 - 0.487Ta - 0.0289Ta^2 \quad (13)$$

Fig. 6 shows the changes of the aspect ratio with Tadaki number along with Eqs. (12) and (13). As can be seen from Fig. 6, when Ta < 0.5, the aspect ratio is distributed around 0.95, and the droplet remains spherical. When Ta > 0.5, the aspect ratio decreases with the increase of the Tadaki number. In yield stress fluids, the Tadaki and Maeda correlation, Eq. (12), generally overestimates the data, while Myint correlation underestimates the data. The consistency between correlation and experimental data is poor.

In addition, some researchers used the Weber number to calculate the aspect ratio. *Taylor* and *Acrivos* [9] expressed the aspect ratio of a droplet in a Newtonian fluid as:

$$E = \sqrt{1 - \frac{9}{16}We} \quad (14)$$

Albert et al. [31] studied the rise dynamics of high-viscosity droplets in a viscous Newtonian liquid. A simple correlation between the aspect ratio and Weber number is given :

$$E = 1 - 0.0773We^{0.92} \quad (15)$$

Fig. 7 shows the changes in the aspect ratio with Weber number along with Eqs. (14) and (15). The existence of yield stress in the Carbopol solution makes the droplet move at a low speed, so the Weber number range of the experiment is extremely low. Within this range, the predicted values of Eqs. (14) and (15) are too high to accurately reflect the changes in aspect ratio with Weber number within the experimental range.

From the comparisons in Figs. 5, 6, and 7, the present data could not be correlated satisfactorily in terms of either the Weber number, Eötvös number, or Tadaki number. Although Wellek's correlation showed a similar trend to the experimental data, Eötvös number represented the ratio of gravitational force to surface tension force, excluding the viscosity term, and the viscosity of Carbopol solutions with different concentrations was significantly different, leading to a small calculation result. *Dong et al.* [32] proposed that a dimensionless number IL (IL = ReEo) was used to characterize the influence of inertia, viscosity, and surface tension on bubble shape when studying the motion of bubbles in ionic liquids. Combined with the experimental data, a new correlation based on the modified dimensionless parameter IL^* ($IL^* = Re^*Eo^*$) was proposed, in the form of

$$E = \frac{1}{1 + 0.125\left(IL^*\right)^{0.78}} \quad (16)$$

The calculation results of Eq. (16) are compared with the experimental data of the four systems, and the results are shown in Fig. 8. It has a higher amount of density of data points using the new dimensionless parameter IL^* than that with Eötvös number, Weber number, and Tadaki number. The mean of the residual sum of squares of the fitting results is 0.006, and $R^2 = 0.802$. With the increase

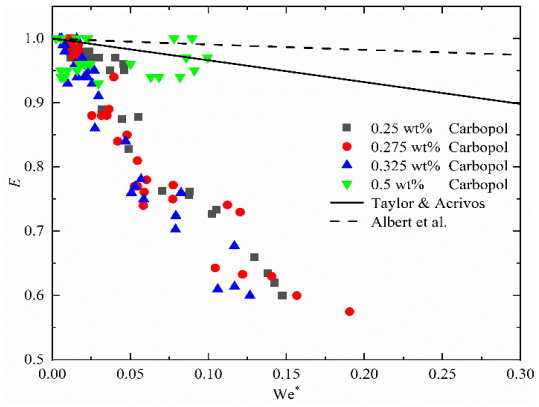

Fig. 7: Comparison of measured aspect ratio values with calculated values vs. Weber number.

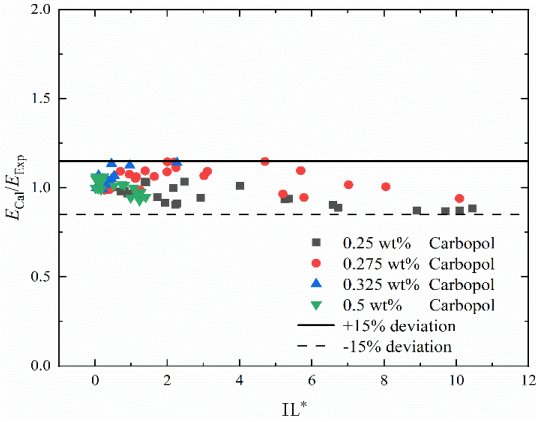

Fig. 9: Measured aspect ratio vs. calculated aspect ratio from Eq. (16) in yield stress fluid.

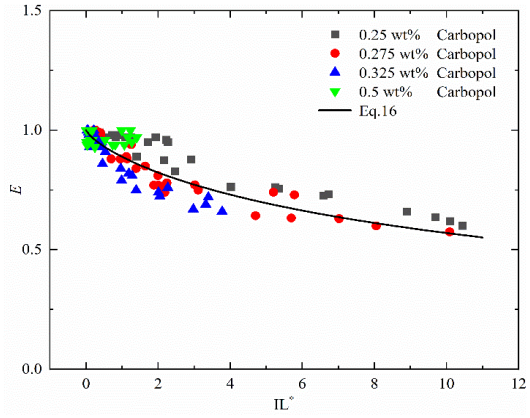

Fig. 8: Relationship between aspect ratio and dimensionless parameter IL*.

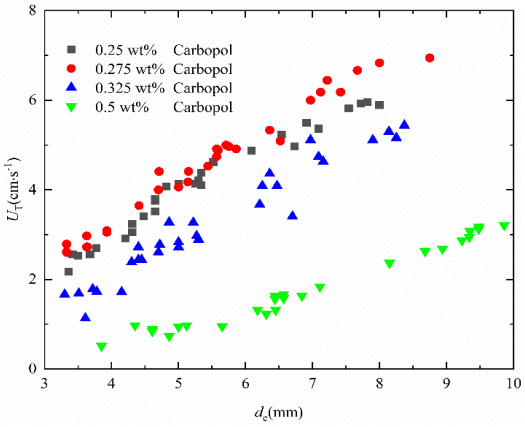

Fig.10: Terminal velocity of the droplet in different yield stress fluids.

of solution concentration, the yield stress, and viscosity of the system increase, which increases the drag force of droplet movement and intensifies the droplet shape change. The results are also shown in Fig. 9. The error range between the experimental value and the predicted value is about 15%, indicating that the prediction model has good applicability to yield stress fluid.

Droplet velocity and drag coefficient

After the droplet is separated from the nozzle, it accelerates upward and finally reaches a stable state. At this time, the velocity of the droplet is the terminal velocity. Fig. 10 shows the change of droplet terminal velocity with equivalent diameter in Carbopol solutions of different concentrations. It can be seen that when the equivalent diameter is the same, the droplet terminal velocity decreases with the increase of solution concentration. This is because the high concentration of Carbopol solution has a high viscosity and yield stress, which reduces the terminal velocity. When the yield stress is the same, the droplet terminal velocity increases with the increase of equivalent diameter. In addition, when the droplet moving speed is small, the Reynolds number is relatively small, and the inertia has little influence on the droplet's rising speed. When the terminal velocity is the same, the droplet diameter in the low-concentration system is smaller. Therefore, in low Reynolds number yield stress fluid, yield stress is the main factor affecting droplet velocity.

When the droplet rises in a steady state, the forces acting on it are mainly buoyancy, gravity, and drag force, according to Newton's second law [32]:

$$(\rho_C-\rho_D)g\frac{\pi d_e^3}{6}=\frac{1}{2}C_D\rho_C U_T^2\frac{\pi d_e^2}{4} \quad (17)$$

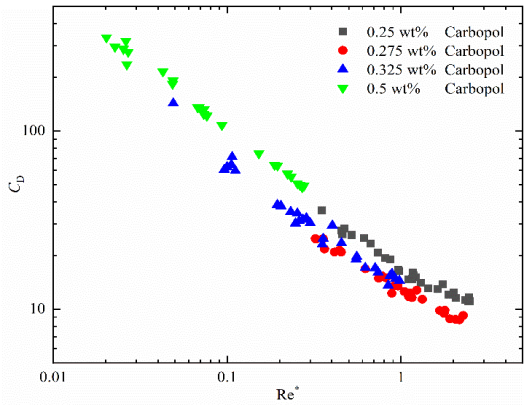

Fig.11: Correlation of drag coefficient as a function of Reynolds number in different yield stress fluids.

The drag coefficient is:

$$C_D = \frac{4d_e g(\rho_C - \rho_D)}{3U_T^2 \rho_C} \tag{18}$$

Fig. 11 shows the change of droplet drag coefficient with Reynolds number in Carbopol solutions of different concentrations. It can be seen that the droplet drag coefficient gradually decreases with the increase of Reynolds number. The shape change of the droplet increases the drag of the droplet due to the large degree of deformation of the droplet in the 0.25 wt% Carbopol solution. The viscosity and yield stress of 0.5 wt% Carbopol solution is larger, and the drag of droplets is larger, so the drag coefficients of 0.25 wt% Carbopol solution and 0.5 wt% Carbopol solution are larger.

By introducing the viscosity ratio and Reynolds number, Hadamard [33] first theoretically derived the drag coefficient expression of a single spherical particle at a low Reynolds number (Re << 1). For bubbles, the viscosity ratio is approximately 0; For rigid solid spheres, the viscosity ratio tends to infinity.

$$C_D = \frac{8}{Re}\left(\frac{2+3\lambda}{1+\lambda}\right) \tag{19}$$

Kishore et al. [19] studied droplet motion in power-low fluids. They discussed the influence of Reynolds number, viscosity ratio, and power-law index on drag coefficient, and proposed the correlation of drag coefficient:

$$C_D = \frac{2}{\lambda+1.85}\left[1.55\lambda\left(\frac{2^{n+2.6}}{Re^{1.36}} + \frac{2^n}{Re^{0.38}}\right) + 1.55\frac{2^{n+2}}{Re^{0.78}}\right] \tag{20}$$

Saboni et al. [20] investigated the motion particles in Newtonian fluids numerically. The results show that the drag coefficient of the droplet decreases with the increase of Reynolds number as the viscosity ratio is fixed. When the Reynolds number is fixed, the drag coefficient of the droplet decreases with the increase in viscosity ratio, and the limit value is the drag coefficient of solid spherical particles. The correlation of the drag coefficient is:

$$C_D = \left\{\left[\lambda\left(\frac{24}{Re} + \frac{4}{Re^{1/3}}\right) + \frac{14.9}{Re^{0.78}}\right] + 40\left(\frac{3\lambda+2}{Re}\right) + 15\lambda + 10\right\}\left[(1+\lambda)\left(5+Re^2\right)\right]^{-1} \tag{21}$$

Under the condition of low Reynolds number ($0 < Re < 2$), the correlation of the droplet drag coefficient of *Oliver* and *Chung* [21] is

$$C_D = \frac{8}{Re}\left(\frac{2+3\lambda}{1+\lambda}\right) + 0.4\left(\frac{2+3\lambda}{1+\lambda}\right)^2 \tag{22}$$

Feng et al. [22] used the finite-difference method to solve the N-S equation of the viscous ball in fluids of different properties, analyzed the influence of Reynolds number and viscosity ratio on the drag force of the ball, and gave the correlation of drag coefficient under specific conditions ($Re \le 5$, $\lambda \le 1.4$):

$$C_D = \frac{26.5}{Re^{0.78}}\left[\frac{(1.3+\lambda)^2 - 0.5}{(1.3+\lambda)(2+\lambda)}\right] \tag{23}$$

These typical and significant correlations described above were selected, namely Eqs. (20) - (23). The results are shown in Fig. 12, which shows the ratio between the calculated and experimental drag coefficient *vs.* the Reynolds number. The experimental drag coefficient in the Carbopol solution differs greatly from the calculated value, because most of the existing criterion correlations are for Newtonian fluids or shear-thinning fluids, and the influence of yield stress on droplet motion is not considered. Therefore, the above correlation cannot be directly applied to yield stress fluid, and the correlation of droplet drag coefficient in yield stress fluid should be established.

The change in droplet shape affects the drag force on the droplet to a certain extent, and the critical Reynolds number during droplet deformation is closely

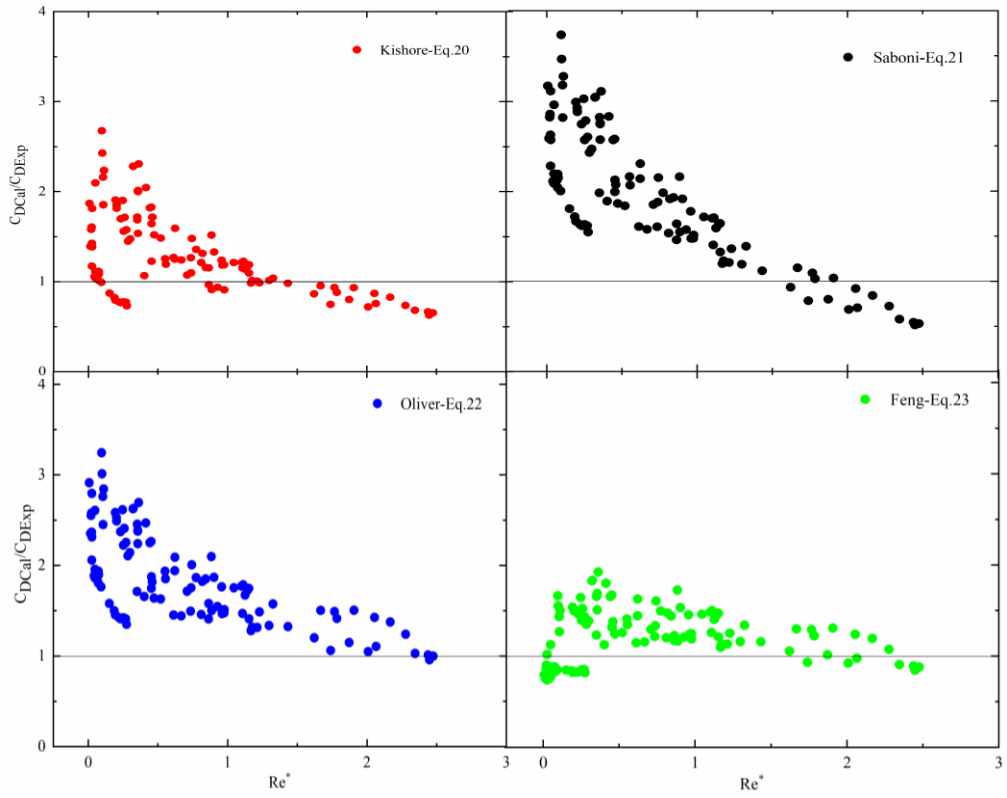

Fig. 12: Predictions of drag coefficient using available models as a function of Reynolds number.

related to the properties of the fluid. Therefore, when predicting the droplet drag coefficient, the influence of droplet deformation and non-Newtonian properties of the fluid should be considered comprehensively. The correlation of Hadamard is modified by introducing the dimensionless number IL^*, combined with the modified Reynolds number, viscosity ratio, a new drag coefficient model $C_D = f(Re^*, \lambda, IL^*)$ is proposed:

$$C_D = \frac{8}{Re^*}\left(\frac{2+3\lambda}{1+\lambda}\right)\left[0.291 + 0.292\ln(IL^* + 1.429)\right] \quad (24)$$

Fig. 13 shows that Eq. (24) is in good agreement with the experimental value. It can be seen that experimental values in 0.25 wt% and 0.5 wt% Carbopol solution are higher than the predicted results of Eq. 24 in the range of $0 < IL^* < 2$, which may be attributed to the severe deformation and high yield stress. Therefore, the deviation of the drag coefficient appears in the range of low IL*. Nevertheless, considering the complexity of the rheological properties of the continuous phase, the deviation is acceptable. Fig. 14 shows the calculated drag coefficients as a function of experimental drag coefficients. All of the data points are between 20% of the calculation. It should be noted that rheological measurement and image processing errors can affect the accuracy of the calculation. When the experimental Reynolds number is large or the droplet surface oscillates violently, the accuracy of the prediction results will be reduced.

CONCLUSIONS

The single droplet rising in yield stress fluids was investigated experimentally. The droplet shape and velocity were obtained by analyzing the images frame-by-frame using MATLAB with a self-written code. The droplet shape changes as follows: the droplet changes from spherical to ellipsoid with the increase of solution concentration in 0.25 wt%, 0.275 wt%, and 0.325 wt% Carbopol solution. The increase of consistency coefficient shows that the solution viscosity increases and the joint action of viscosity force and yield stress causes the droplet shape to change. The viscous forces and yield stresses limit

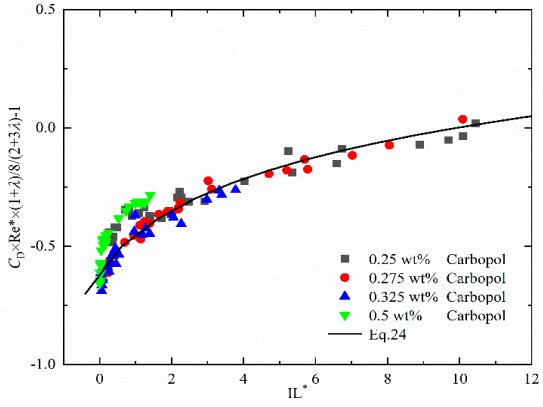

Fig.13: Drag coefficient vs. dimensionless parameter IL*.

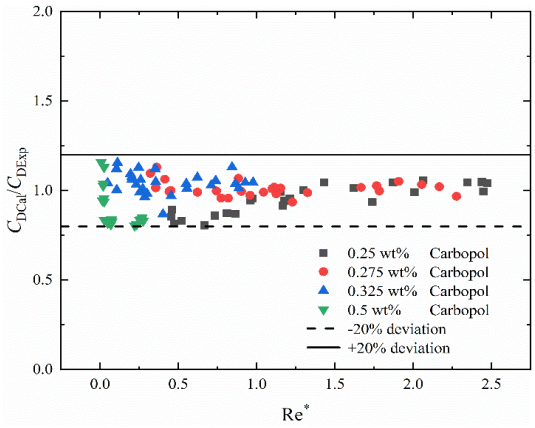

Fig. 14: The ratio of the calculated and experimental drag coefficients as a function of Reynolds number in different yield stress fluids.

the lateral tensile of the droplet, and the droplet shows a spherical shape in 0.5 wt% Carbopol solution. Moreover, the lower droplet velocity results in lower shear dilution, so the power-law index has little influence on droplet shape change. After verification, it is found that the correlation of droplet aspect ratio given in the literature has a large error. The aspect ratio decreases and the droplet shape changes from spherical to ellipsoid with the increase of Eötvös number, Tadaki number, and Weber number. However, the droplet shape has no obvious change and remains spherical with the increase of Bingham number. The droplet shape in yield stress fluid predicted by a single dimensionless number is not satisfactory. Based on experimental data, the correlation of droplet aspect ratio in yield stress fluid was given, and the predicted droplet aspect ratio is in good agreement with experimental results (the error is less than 15%). The terminal velocity of the droplet increases with the increase of diameter and the decrease of continuous liquid concentration. The larger the yield stress is, the smaller the droplet terminal velocity is. It is found that the existing drag coefficient correlation is not suitable for a droplet in yield stress fluid. Combined with the experimental data, a new drag coefficient correlation $C_D = f(Re^*, \lambda, IL^*)$ was established. The predicted results are in good agreement with the experimental values. The correlation can more accurately reflect the real motion of the droplet.

Appendix A

```
pic_ref = imread('0.bmp');
photo = dir('*.bmp');
for i = 2:length(photo)-1
pic1 = imread(photo(i).name);
pic2 = imread(photo(i+1).name);
%pic(xx:xx,xx:xx) = xx;
area1 = pic_ref(y_range,x_range)-pic1(y_range,x_range);
%area(xx,xx) = xx;
area1 = imfill(area1);
area2 = pic_ref(y_range,x_range)-pic2(y_range,x_range);
%area(xx,xx) = xx;
area2 = imfill(area2);
thr1 = 0.45*max(max(area1));
area1 = area1-thr1;
area1 = imfill(area1);
thr2 = 0.45*max(max(area2));
area2 = area2-thr2;
area2 = imfill(area2);
M = length(y_range);

%Determine the geometric center of the droplet to be analyzed
%for j = 1:M
%col = find(area1(j,:) > 0);
%if length(col) > 0
%xc(j) = (x_range(col(1))+x_range(col(length(col))))/2;
%yc(j) = y_range(j);
%else
%xc(j) = 0;
%yc(j) = 0;
%end
%end
%ind = find(xc>0);
%x1 = sum(xc)/length(ind);

%y1 = sum(yc)/length(ind);
%ind = find(yc>0);
```

```
[row,col] = find(area1 > 0);
x1 = mean(x_range(col));
y1 = mean(y_range(row));

%Determine the geometric center of the droplet to be
referenced
%for j = 1:M
%col = find(area2(j,:) > 0);
%if length(col) > 0
%xc(j) = (x_range(col(1))+x_range(col(length(col))))/2;
%yc(j) = y_range(j);
%else
%xc(j) = 0;
%yc(j) = 0;
%end
%end
%ind = find(xc>0);
%x2 = sum(xc)/length(ind);
%ind = find(yc>0);
%y2 = sum(yc)/length(ind);
[row,col] = find(area2 > 0);
x2 = mean(x_range(col));
y2 = mean(y_range(row));

v(i-1) = scale*sqrt((x2-x1)^2+(y2-y1)^2)/delta;
theta(i-1) = atan((x2-x1)/(y1-y2));
vx(i-1) = scale*(x2-x1)/delta;
vz(i-1) = scale*(y1-y2)/delta;

x(i-1) = (x1-x_ref)*scale;
y(i-1) = (y_ref-y1)*scale;
end
x = x';
y = y';
v = v';
theta = theta';
vx = vx';
vz = vz';
dropletvelocity = [x y v theta vx vz];
save dropletvelocity.txt droplet velocity -ascii
```

Nomenclature

Bn	Bingham number, $Bn=\tau_0 d_e/\mu U_T$, dimensionless
Bn^*	Modified Bingham number, dimensionless
C_D	Drag coefficient
d_e	Volume equivalent droplet diameter, mm
E	Aspect ratio
Eo	Eötvös number, $Eo=(\rho_C-\rho_D)gd_e^2/\sigma$, dimensionless
Eo^*	Modified Eötvös number, dimensionless
g	Gravitational acceleration, m/s^2
IL	Characterizes inertia, viscosity, and surface tension, dimensionless
IL^*	Modified parameters $IL^*=Re^*Eo^*$, dimensionless [-]
k	Consistency coefficient ($Pa\cdot s^n$)
Mo	Morton number, $Mo=(\rho_C-\rho_D)g\mu_C^4/(\sigma^3\rho_C^2)$, dimensionless
n	Index in power-law model
Re	Reynolds number, $Re=\rho_C d_e U_T/\mu$, dimensionless
Re^*	Modified Reynolds number, dimensionless
Δt	The time interval between two consecutive images, s
Ta	Tadaki number, $Ta=ReMo^{0.23}$, dimensionless
Ta^*	Modified Tadaki number, $Ta=Re^*Mo^{*0.23}$ dimensionless
U_b	Local velocity, cm/s
U_T	Terminal velocity, cm/s
V	Droplet size, mm^3
We	Weber number, $We=\rho_C d_e U_T^2/\sigma$, dimensionless
We^*	Modified Weber number, dimensionless
y_i	The center of gravity of the droplet at the previous moment, cm]
y_{i+1}	The center of gravity of the droplet at the latter moment, cm
Y	Drag coefficient factor

Greek symbol

$\dot{\gamma}$	Shear rate, s^{-1}
λ	Viscosity ratio of the dispersed phase to the continuous phase
μ	Viscosity, Pa·s
ρ	Density, kg/m^3
$\Delta\rho$	Density difference, kg/m^3
σ	Surface tension, mN/m
τ_0	Yield stress, Pa

Subscripts

C	Continuous phase
D	Dispersed phase

Acknowledgments

The authors thank the National Natural Science Foundation of China (21406141) and the Natural Science

Foundation of Liaoning Province (2019-MS-252) for their financial support.

Received : Dec. 30, 2021 ; Accepted : Apr. 4, 2022

REFERENCES

[1] Shima E.R., Shahab G., Ali A.S., Ali R.B., Mostafa G.G., Experimental Study on Enhanced Oil Recovery by Low Salinity Water Flooding on the Fractured Dolomite Reservoir, *Iran. J. Chem. Chem. Eng. (IJCCE)*, **40(5)**: 1703-1719 (2021).

[2] Anil C.R., Suresh V.R., Cyrus K.M., Selective Oxidation of Lauryl Alcohol to Lauraldehyde under Liquid-Liquid Phase Transfer Catalysis (LL-PTC) with Potassium Chromate as the Oxidizing Agent, *Iran. J. Chem. Chem. Eng. (IJCCE)*, **37(6)**: 89-94 (2018).

[3] Kouissi T., Bouanz M., Ouerfelli N., KCl-Induced Phase Separation of 1,4-Dioxane + Water Mixtures Studied by Electrical Conductivity and Refractive Index, *J. Chem. Eng. Data*., 54: 566-573 (2009).

[4] Majid M., Babak A., Ashkan G., Liquid-Liquid Extraction in a Microextractor: A Laboratory Examination and Thermodynamic Modeling of N-Hexane + Benzene + Sulfolane System, *Iran. J. Chem. Chem. Eng. (IJCCE)*, **40(2)**: 657-666 (2021).

[5] Zhang J.Y.Z., Wang Y.D., Stevens G.W., Fei W.Y., An Experimental Study on Single Drop Rising in a Low Interfacial Tension Liquid–Liquid System, *Chem. Eng. Res. Des.*, **148**: 349-360 (2019).

[6] Bäumler K., Wegener M., Paschedag A.R., Bänsch E., Drop Rise Velocities and Fluid Dynamic Behavior in Standard Test Systems for Liquid/liquid Extraction-Experimental and Numerical Investigations, *Chem. Eng. Sci.*, 66(3): 426-439 (2011).

[7] Eiswirth R.T., Bart H.J., Atmakidis T., Kenig E.Y., Experimental and Numerical Investigation of a Free Rising Droplet, *Chem. Eng. Process.*, **50(7)**: 718-727 (2011).

[8] Wegener M., Kraume M., Paschedag A.R., Terminal and Transient Drop Rise Velocity of Single Toluene Droplets in Water, *AIChE J.*, **56(1)**: 2-10 (2010).

[9] Taylor T.D., Acrivos A., On the Deformation and Drag of a Falling Viscous Drop at Low Reynolds Number, *J. Fluid Mech.*, **18(3)**: 466-476 (1964).

[10] Wairegi T., Grace J.R., The Behavior of Large Drops in Immiscible Liquids, *Int. J. Multiphase Flow*, **3(1)**: 67-77 (1976).

[11] Liu L.L., Tang H., Quan S.P., Shapes and Terminal Velocities of a Drop Rising in Stagnant Liquids, *Comput. Fluids*, **81**:17-25 (2013).

[12] Fakhari A., Rahimian M.H., Investigation of Deformation and Breakup of a Falling Droplet Using a Multiple-Relaxation-Time Lattice Boltzmann Method, *Comput. Fluids*, **40(1)**: 156-171 (2011).

[13] Wegener M., Fevre M., Paschedag A.R., Kraume M., Impact of Marangoni Instabilities on the Fluid Dynamic Behaviour of Organic Droplets, *Int. J. Heat Mass Tran.*, **52(11-12)**: 2543-2551 (2009).

[14] Jie Y., Fei W.Y., Li H.Z., Effect of Packing on Drop Swarms Extraction of High Viscosity Solvents, *Hydrometallurgy*, **78(1-2)**: 30-40 (2005).

[15] Beris A.N., Tsamopoulos J.A., Armstrong R.C., Brown R.A., Creeping Motion of a Sphere Through a Bingham Plastic, *J. Fluid Mech.*, **158(-1)**: 219-44 (1985).

[16] Dubash N., Frigaard I.A., Propagation and Stopping of Air Bubbles in Carbopol Solutions, *J. Non-Newtonian Fluid.*, **142(1-3)**: 123-134 (2007).

[17] Lavrenteva O.M., Hollenberg Y., Nir A., Motion of Viscous Drops in Tubes Filled with Yield Stress Fluid, *Chem. Eng. Sci.*, **64**: 4772–4786 (2009).

[18] Sarabian M., Rosti M.E., Brandt L., Hormozi S., Numerical Simulations of a Sphere Settling in Simple Shear Flows of Yield Stress Fluids, *J. Fluid Mech.*, **896**: A17 (2020).

[19] Kishore N., Chhabra R.P., Eswaran V., Drag on a Single Fluid Sphere Translating in Power-law Liquids at Moderate Reynolds Numbers, *Chem. Eng. Sci.*, **62(9)**: 2422-2434 (2007).

[20] Saboni A., Alexandrova S., Numerical Study of the Drag on a Fluid Sphere, *AIChE J.*, **48(12)**: 2992-2994 (2002).

[21] Oliver D.L.R., Chung J.N., Flow about a Fluid Sphere at Low to Moderate Reynolds Numbers, *J. Fluid Mech.*, **154(-1)**: 1-18 (1985).

[22] Feng Z.G., Michaelides E.E., Drag Coefficients of Viscous Spheres at Intermediate and High Reynolds Numbers, *J. Fluid Eng.*, **123(4)**: 841-849 (2001).

[23] Sikorski D., Tabuteau H., Bruyn J.R., Motion, and Shape of Bubbles Rising Through a Yield-Stress Fluid, *J. Non-Newtonian Fluid Mech.*, **159**: 10–16 (2009).

[24] Stokes J.R., Telford J.H., Measuring the Yield Behaviour of Structured Fluids, *J. Non-Newtonian Fluid Mech.*, **124**: 137–146 (2004).

[25] Atapattu D.D., Chhabra R.P., Uhlherr P., Wall Effect for Spheres Falling at Small Reynolds Number in a Viscoplastic Medium, *J. Non-Newtonian Fluid.*, **38(1)**: 31-42 (1990).

[26] Nirmalkar N., Chhabra R.P., Poole R.J., Numerical Predictions of Momentum and Heat Transfer Characteristics from a Heated Sphere in Yield-Stress Fluids, *Ind. Eng. Chem. Res.*, **52(20)**: 6848–6861 (2013).

[27] Clift R., Grace J.R., Weber M.E., Bubbles, drops, and particles. Academic Press, New York USA, (1978).

[28] Wellek R.M., Agrawal A.K., Skelland A.H.P., Shape of Liquid Drops Moving in Liquid Media, *AIChE J.*, **12(5)**: 854-862 (1996).

[29] Tadaki T., Maeda S., On the Shape and Velocity of Single Air Bubbles Rising in Various Liquids, *Chem. Eng.*, **25(4)**:254-264 (1961).

[30] Myint W., Hosokawa S., Tomiyama A., Shapes of Single Drops Rising Through Stagnant Liquids, *J. Fluid Sci. Technol*, **2(1)**:184-195 (2007).

[31] Albert C., Kromer J., Robertson A.M., Bothe D., Dynamic Behavior of Buoyant High Viscosity Droplets Rising in a Quiescent Liquid, *J. Fluid Mech.*, **778**: 485-533 (2015).

[32] Dong H.F., Wang X.L., Liu L., Zhang X.P., Zhang S.J., The Rise and Deformation of a Single Bubble in Ionic Liquids, *Chem. Eng. Sci.*, **65(10)**:3240-3248 (2010).

[33] Hadamard J.S., Movement Permanent Lent D'une Sphère Liquide et Visqueuse Dans un Liquide Visqueux, *Comp. trend. Acad. Sci. Paris*, **152**: 1735-1738 (1911).